RGNZ/MGPB

# Improving the quality of silica sand as a proppant for hydraulic fracking industry purposes

Rudarsko-geološko-naftni zbornik
(The Mining-Geology-Petroleum Engineering Bulletin)
UDC: 622.276
DOI: 10.17794/rgn.2025.1.11

Original scientific paper

**Suzan S. Ibrahim[1]*; Tawfik R. Boulos[1]; Sameh M. Abdullah[2]; Abdalla M. Elbendari[1]; Mohamed G. Khalifa[2]; Ayman A. Hagrass[2]**

[1]*Central Metallurgical Research and Development Institute (CMRDI) P.O. Box 87, Helwan 11421, Egypt.*
[2]*Tabbin Institute for Metallurgical Studies (TIMS) P.O. Box 109, Helwan 11421, Egypt.*

**Abstract**

A technological silica sand sample that belongs to "Egypt's Future Quarries", south west Cairo, was investigated as a proppant for the hydraulic fracking industry. The sample showed encouraging physical and mechanical characteristics, yet it was still in need of improving its grade to match the International Organization for Standardization specifications. After careful reading of the microscopy and mineralogy investigation of the head sample, a simple and cheap beneficiation flowsheet was suggested including sieve classification and an attrition scrubbing technique using a 50-liter capacity "Denver" machine. The results showed appreciable grade improvement in the attrition sand. An increase in silica content from 90.10% to 98.15% $SiO_2$ at the expense of alumina and iron oxides %'s by 79% and 63%, respectively. This grade improvement subsequently led to notable improvement in turbidity and acid solubility measures and hence, transformed the sand sample from being unacceptable for the oil and gas industry to a sand product with acceptable specifications for this industry. The results also showed improvement in the crushability resistance and grain sphericity and roundness measures with ratios reaching 24.06%, 19.11% and 16.72%, respectively. In addition, particle size distribution of the attrition sand showed more consistency, which is desirable for the fracking industry.

**Keywords:**
hydraulic fracking industry; proppants specifications; silica sand; attrition scrubbing

## 1. Introduction

Silica sand is a highly versatile non-metallic mineral, primarily composed of high-purity quartz grains that give it a distinctive white color. It is a critical material in various industries, including glassmaking, foundry work, abrasives, filtration, ceramics, refractories, coatings, fillers, silicon-based chemicals, and hydraulic fracturing. The properties of silica sand, such as its purity, grain size, and chemical composition, vary depending on its intended use. These characteristics affect its performance in applications ranging from glass and ceramics to industrial sand for filtration and refractories (**Nigussie et al., 2023; Silica Sand Global Market Report, 2024**).

Economic analyses have highlighted the significant impact of silica sand on various industries. For instance, the hydraulic fracturing (fracking) industry alone has an economic impact of $100 million, with demand fluctuations showing a ±20% variation. High demand scenarios can increase this impact to $120 million, while low demand scenarios reduce it to $80 million. This sensitivity underscores the importance of the fracking sector in the broader economic implications of silica sand, making it a key focus for understanding the mineral's value (**Fitzgerald, 2012; US Geological Survey, 2024; Imarc, 2024**). The global market for silica sand was valued at USD 24.2 billion in 2023 and is expected to grow to USD 37.6 billion by 2032, reflecting a compound annual growth rate (CAGR) of 4.9%. The frac sand market, driven by increased exploration and reliance on unconventional hydrocarbon resources, was valued at $7.6 billion in 2023 and is projected to reach $14 billion by 2027 (**Powder and Bulk Solids, 2019**). The U.S. proppant market, including frac sand, was valued at $3,653 million in 2022 and is expected to grow at an annual rate of 8.04% to reach $6,105.5 million by 2028 (**Research and Markets, 2024**). For silica sand to be economically viable as a proppant, its beneficiation costs must be lower than transportation costs from the quarry to the well site. Beneficiation processes typically include the washing and separation of gangue minerals. As processing techniques become more complex, the cost of beneficiation increases (**Fuerstenau and Han, 2003; Ibrahim et al., 2018; Abdullah, 2020; Arslan, 2021; Gaber and Gamal El-Din, 2021**).

Hydraulic fracturing, or "fracking," involves injecting water, sand (or other proppants), and chemicals at

* Corresponding author: Suzan S. Ibrahim
*e-mail address: suzansibrahim@gmail.com*

**Figure 1:** Field photographs for the studied area

high pressure into bedrock formations to create and enhance fractures. This technique is essential for stimulating wells in low-permeability rocks like tight sandstone, shale, and coal beds to increase oil and gas flow (**US Geological Survey, 2024**). Proppant grain sizes typically range from 20/40 to 40/70 mesh, with sizes determined by ASTM D6913 standards (**Gu et al., 2015; Liang et al., 2016; Zheng et al., 2018**). Proppant particle shape and size distribution are important because they affect how the particles pack within the fracture. In addition, the density is important because, for any given proppant particle shape and size, a particle of lower density is easier to transport deeper into a fracture without settling. On the other hand, the mechanical strength of proppants is critical, as it measures their ability to resist crushing under pressure. Crush resistance and breakage ratio are key parameters, with proppants needing a breakage ratio of less than 10% to effectively withstand formation closure pressures (**Zoviedavianpoor and Gharibi, 2016; Mocciaro et al., 2018; API 19C, 2008**). In general, proppants suitable for formations with closure pressures between 40 and 50 MPa is being preferred (**O'Driscoll, 2013**). Acid resistance is an important property in proppants, because greater acid resistance means greater robustness under chemical exposures that the proppant grains may face during the hydraulic fracturing operation. The interaction and the different effective parameters like temperature, soaking time, static and dynamic conditions between mud acid (a mixture of hydrochloric: hydrofluoric acids with 12: 3 by mass) and sand proppant were studied (**Assem and Nasr-El-Din, 2015**).

Silica sand used in fracking must meet stringent quality standards set by the International Organization for Standardization (**ISO 9001:2015**), which include high silica content, narrow grain size distribution, low acid solubility (2% or less), low turbidity (250 FTU/NTU or less), high crush resistance (10% or more), and grain sphericity and roundness of 0.6 or higher. Other important properties include low bulk density for flowability, and appropriate grain size, which affects fracture conductivity are required. However, each fracking operation requires approximately 1,000 tons of frac sand, and the demand for this material is expected to remain high.

In Egypt, vast reserves of high-quality silica sand are underutilized. While the price of frac sand has increased from $26.5 per ton in 2022 to over $70.5 per ton during shortages, identifying suitable local sources could reduce transportation costs and improve efficiency (**Wahab et al., 2022**). Research is ongoing to assess the suitability of silica sand from Egypt's "Future Quarries" project for hydraulic fracturing. Initial evaluations showed promising physical and mechanical properties, though the chemical grade did not meet international standards. Proposed beneficiation processes, including screen classification and attrition scrubbing, have improved the silica grade and other chemical characteristics, making the sand acceptable as a proppant. This research demonstrates the potential for improved fracking operations using locally sourced silica sand.

## 2. Materials and methods

A one-ton technological silica sand sample was supplied from the "Egypt's Futurer Quarries" Company. The studied area extends from 6$^{th}$ of October city, northwest of Giza State to Siwa Oasis. It is located between latitude of 30°01'12''N and longitude of 30°49'51''E, (see **Figure 1** and **Figure 2**). It was taken into account that the sample was collected in a correct geological way, so that the entire deposit area was well represented by the taken sample. Then the entire amount of sand was

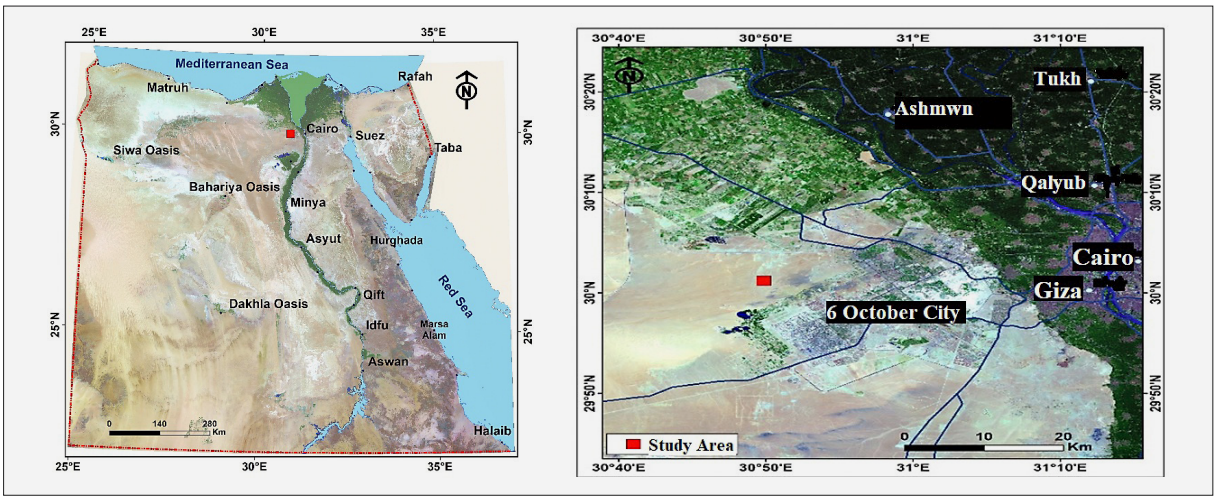


**Figure 2:** Egypt's futurer quarries, Long: 30°49'51"E, Lat: 30°01'12"N

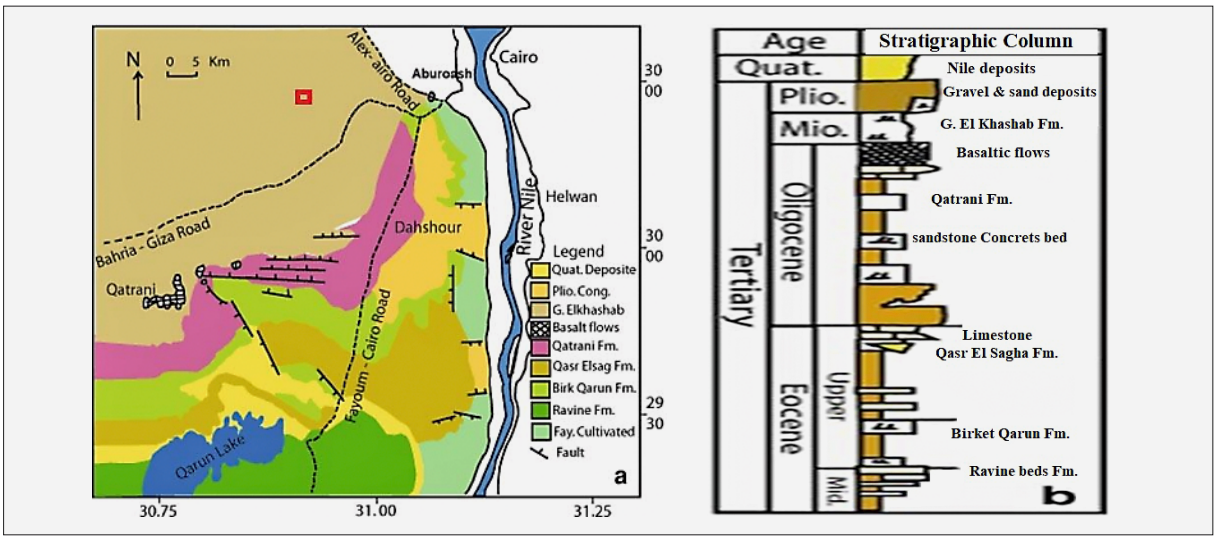


**Figure 3:** Geological map of the studied area, north Western Desert of Egypt (**Abdel Kader et al., 2013**)

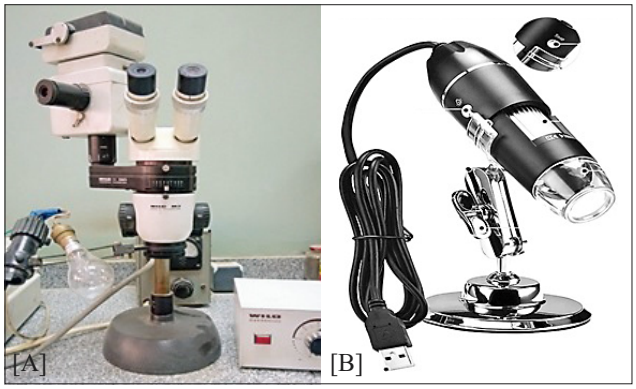


**Figure 4:** [A] Wild Heerbrugg M3 stereo microscope, [B] Mega Pixels 1600x microscope

mixed well and subjected to a successive mixing and quartering technique to collect about 1 ton of the sample. The geological map of the studied area is shown in (see **Figure 3**). From a geological point of view, the continental crust (upper part of basement surface) has a major sedimentary basin which has a wide extension and probably extends further outside of the investigated area. The geological studies of the area showed that a simple geologic structure affects the relatively thick cover of younger sediments (**Abdel Kader et al., 2013**).

Exploratory tests showed promising results of the sample. However, the sample was still in need of improving its quality to match rigid specifications for hydraulic fracturing industry. A simple beneficiation flowsheet was suggested to reach this target. This includes dry screen classification to reject fractions of coarse +850 microns and fine -106 microns. The dry classified product of -850+106 microns was then subjected to a multi-staged attrition scrubbing process using a 50 Liter "Denver" attrition unit at a spindle speed of 900 rpm and maximum pulp density reaching 70-72% for 15 minutes. This period took place in three equal and consecutive stages of time. Each attrition step was followed by thorough water washing and desliming on 106 microns vibrating "Russell" screening before beginning

the new attrition step. At the end of the process, all the attrition products were collected separately, dried, weighed and evaluated.

Sample characterization was conducted through mineralogy microscope investigation using Wild Heerbrugg M3 stereo microscope Typ 352873, Switzerland. Mega Pixels 1600x 8 Led digital electronic microscope was adapted to measure sphericity and roundness of sand grains, (see **Figure 4**). In addition, chemical analysis was applied using a Panalytical-Axios XRF unit. Where sieve analysis was applied using Fritsch, Analysette and Retsch, GmbH, Germany (**Zheng et al., 2021; Jia et al., 2022**).

### *2.1. Attrition-scrubbing of classified sand*

Attrition scrubbing is an indispensable technology in silica sand processing flow-sheet programs to meet the specifications of glass industries. However, attrition scrubbing machine structural configuration, scrubbing strength and time, slurry concentration and the added chemical medium all have some influence in the scrubbing effect. The slurry concentration can affect the dispersion and friction between particles, and it is necessary to determine the optimized final slurry concentration while only changing the slurry concentration. The added agent affects the scrubbing effect by changing the hydrophilicity of the particle surface and the repulsion between particles.

Attrition is defined as the act of wearing by friction and abrasion as a consequence of attrition. Based on this definition, attrition is the act (loading mechanism) that causes abrasion (breakage mechanism). Generally, the definition of attrition and abrasion is closely related to the shear loading mechanism (**Cleary and Morrison, 2016**). When the attrition machine enters the processing flowsheet, the strong particle-particle friction forces between sand grains and under strong turbulence inside the attrition tank, an effective grain-grain rubbing or abrasion action occurred. This leads to a breakdown of the adhered clayey coatings and ferruginous staining from the sand grains surface. Subsequently, a grade improving in the silica sand sample takes place. Abrasion is characterized by the formation of fines and no noticeable change in the feed particle size distribution. However, when the kinetic energy inside the attrition tank is high enough, chipping breakage, as a special case of cleavage, is experienced. Then sharp edges on the sand surface can break off and weak location cracks in the sand body may show splitting. In contrast to abrasion, chipping showed in general no fines formation, but on the other hand, it leaves behind broken silica fragments in different shapes and sizes. In addition, a notable change in the feed particle size distribution occurred (**Wahab et al., 2022; Abdullah, 2023; Uluosoy, 2023; Ravisankar et al., 2023; Othman et al., 2023; Benmebarek et al., 2023**).

Microscopic investigation of the original sand sample showed that coarse particle +850 microns were mainly composed of large gravels and pebbles granules, where fines below 106 microns were often filled with fine clay materials as well as grains of undesirable heavy and refractory minerals. In accordance, the head sample was subjected to dry classification using 850 microns and 106 microns shaking sieves to reject coarse and fine fractions before delivery to the attrition scrubbing process. However, preparing the sand charge before attrition is important to ensure the highest performance within the washing unit.

Dry classified sand of -850+106 microns was then subjected to a vigorous attrition scrubbing process for 15 minutes. This period took place in three equal and consecutive stages of time. These attrition stages were separated by a good washing process with water and desliming on a 106 microns "Russell" vibrating sieve before starting the new attrition step (**Ibrahim et al., 2013**). The attrition process was conducted using a 50 liter capacity "Denver" attrition scrubbing machine (2 horse power motor) at a spindle speed of 900 rpm and maximum pulp density reaching 70-72% solid (see **Figure 5**). The attrition tank is designed with two cells, each equipped with opposing axial flow propellers that create a high-intensity impact zone between them. A slurry is introduced into the scrubber chamber via a feed pipe from the first cell, where it is directed downward and flows through a gate at the bottom into the second cell. The slurry undergoes intense turbulence due to the vigorous agitation of the propellers. As the slurry moves, each particle undergoes multiple violent impacts with other particles, resulting in their disintegration and the removal of clay and other impurities. These disintegrated impurities and clay become suspended in the slurry and can be subsequently separated through desliming. At the end of the process, all the attrition products were collected separately, dried, weighed and evaluated. The attrition sand sample was subjected to various frac sand testing according to API recommends including turbidity, acid solubility, bulk density, particle size distribution, crushability resistance, sand grains sphericity and roundness (**API 19C, 2008**).

To improve silica grade, the sample has to be clean from silt and ferruginated clayey surface coating matters as well as the most stubborn impure iron oxides films adhering to the sand grains surface. This is in order to pass the turbidity measure to less than 250 Formazin Turbidity Units (FTUs) or Nephelometric Turbidity Unit (NTUs), and the acid solubility measure to less than 2% (**API 19-C, 2008**).

The turbidity measure is very important, where it is an indication of how dirty the frac sand is. However, high silica content with a low clay content of the sand sample contribute to strong brittleness and help hydraulic fracture propagation. In addition, the turbidity test regulations are very important for a better-quality sand to maximize fracturing operations while being safer for the environment and for the workers from inhaling too much silica dust over a long time. However, the lower the turbidity, the better the performance of the proppant (**API 19-C, 2008**). To determine the turbidity test, 50 g of the sand sample was added to a 100 ml of distilled water.

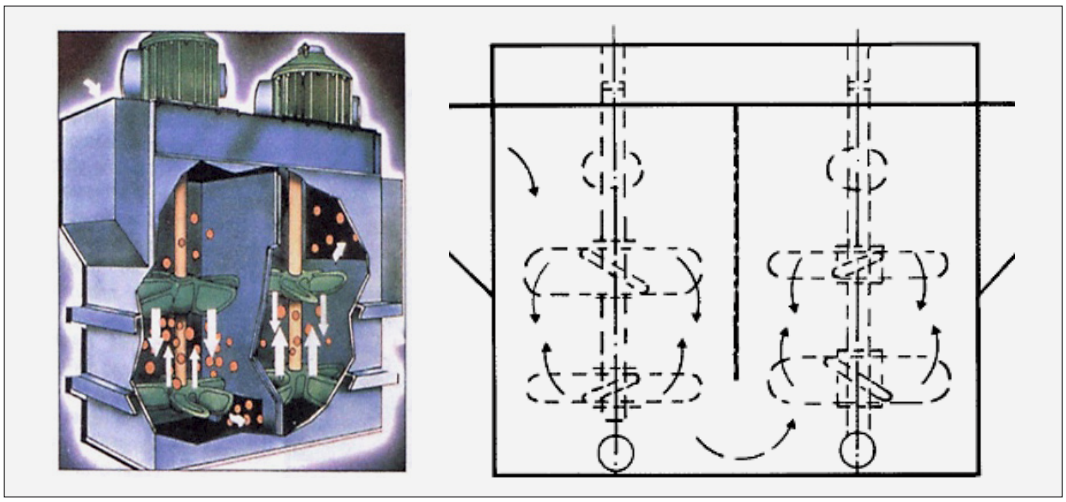

**Figure 5:** 50 liters "Denver" attrition scrubber unit (**Ibrahim et al., 2013**)

The mixture was left for 30 min, then shaken for 30 seconds and left to rest for another 5 min. Twenty-five ml was then extracted using a syringe from the center of the mixture and tested using Micro 1000 turbidimeter (**API 19-C, 2008**).

On the other hand, the acid solubility test determines the suitability of sand for use in applications where it can come into contact with acids during operations. In fact, a good acid resistivity proppant is beneficial for long-term conductivity as this reduces the drop in strength due to the leaching of materials that support the structural integrity of the proppant. The API frac sand specs recommend the maximum percent (%) by weight of the frac sand that can be soluble in acid: 2% or less for frac sand mesh sizes 6/12 through 30/50 and 3% or less for frac sand mesh sizes 40/70 through 70/140 (**API 19-C, 2008**).

The acid solubility test was conducted with a mixture of hydrochloric: hydrofluoric acids (12: 3 by mass). The HF solution was first prepared by dissolving 46.23 g of pure ammonium bi-fluoride in 500 ml of distilled water in a 1000-ml volumetric flask. Then, 361 ml of 37% HCl was added to the solution. The mixture was diluted to 1000 ml with deionized water. While preparing the HCl/ HF solution, 5 g of the sand sample and the filter papers were dried in the oven at 105°C. The mass of the sample with the filter paper was weighed and recorded. The dried sand was added into 100 ml of the HCl/ HF solution, then the mixture was heated in a water bath at 66°C for 30 min. The mixture was rinsed, vacuum-filtered and dried. Finally, the weight of the sample and the filter paper was measured and recorded, where the acid solubility% was calculated (**API 19-C, 2008**).

## 3. Results and discussion

### *3.1. Head sample characterization*

Complete chemical analysis of original sand ore sample is shown in **Table 1**. The results indicated that the sample contained 90.59% $SiO_2$, 3.37% $Al_2O_3$, 1.17% $Fe_2O_3$, 2.14% CaO. In addition to other minor oxides, e.g. 0.55% $SO_3$, 0.37% $Na_2O$, 0.16% $TiO_2$, and 0.27% MgO. Yet the silica sand sample did not match fracking application with respect to its silica grade according to the International Standards. On the other hand, **Tables 2** and **3** illustrate particle size distribution of the original sample as received and the dry classified product of -850+106 microns as well. Particle size distribution of

**Table 1:** Chemical analysis of sand head sample

| Constituent | Wt., % | Constituent | Wt., % |
|---|---|---|---|
| $Na_2O$ | 0.37 | CaO | 2.14 |
| MgO | 0.27 | $TiO_2$ | 0.16 |
| $Al_2O_3$ | 3.37 | MnO | 0.03 |
| $SiO_2$ | 90.59 | $Fe_2O_3$ | 1.17 |
| $P_2O_5$ | 0.19 | CuO | 0.01 |
| $SO_3$ | 0.55 | SrO | 0.01 |
| Cl | 0.13 | $ZrO_2$ | 0.02 |
| $K_2O$ | 0.66 | LOI | 0.33 |

**Table 2:** Particle size distributions of sand head sample

| Particle size, um | Wt., % | Cum. Wt., % Retained |
|---|---|---|
| +850 | 11.10 | 11.10 |
| -850+600 | 33.10 | 44.20 |
| -600+500 | 12.70 | 56.90 |
| -500+425 | 8.40 | 65.30 |
| -425+355 | 8.50 | 73.80 |
| -355+300 | 7.30 | 81.10 |
| -300+250 | 5.00 | 86.10 |
| -250+212 | 2.60 | 88.70 |
| -212+150 | 5.20 | 93.90 |
| -150+106 | 4.64 | 98.50 |
| -106 | 1.46 | 100.00 |

**Table 3:** Particle size distributions of dry classified sand of -850+106 microns

| Particle size, um | Wt., % | Cum. Wt., % Retained |
|---|---|---|
| -850+600 | 37.86 | 37.86 |
| -600+500 | 14.52 | 52.38 |
| -500+425 | 9.61 | 61.99 |
| -425+355 | 9.72 | 70.71 |
| -355+300 | 8.36 | 80.07 |
| -300+250 | 5.72 | 85.79 |
| -250+212 | 2.97 | 88.76 |
| -212+150 | 5.95 | 94.71 |
| -150+106 | 5.29 | 100.00 |

the sand head sample and its dry classified product are illustrated in **Figure 6**. Sand size fractions +850 microns and -106 microns were shown to represent 11.10% and 1.46% by wt., respectively, in **Table 2**. Microscopic investigation of the head sample showed that the size fraction +850 microns was mainly composed of large gravel and colored pebbles grains, where the fines below 106 microns were undesirable for fracking application. However, these two fractions were disposed of in situ and set aside for use in other suitable applications.

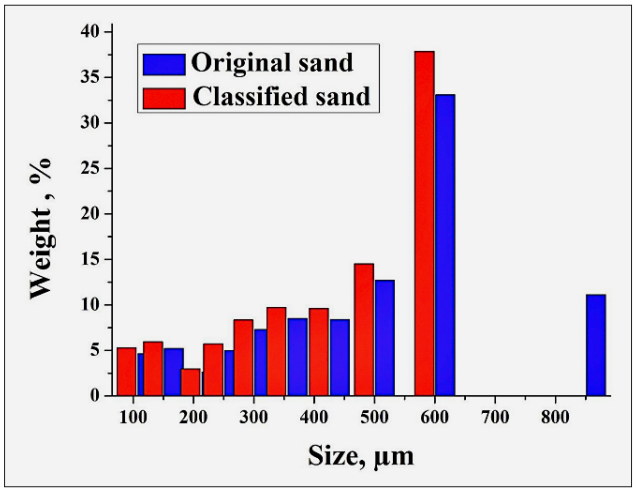


**Figure 6:** Particle size distribution of sand head sample vs classified product

### *3.2. Attrition scrubbing results*

#### *3.2.1. Improved sand sample grade*

Microscope investigation of the sand sample classified as -850+106 microns showed that most of the sand grain surfaces were densely covered with a clayey coating material that tends to be a dark yellow reddish coloration, in addition to colored splashes on some sand grain surfaces (see **Figure 7**). After attrition, the washed sand seemed white in color after getting rid of most colored ferruginated clayey coating material on sand grain surfaces (see **Figure 8**). The over-all under screen tail of -106 microns was about 7.07% by weight of the attrition feed. It was composed of two components. The first one was the muddy coating tailing component that was mostly produced after the first attrition step. It was of a deep yellow-reddish colored muddy material weighing about 4.94% by wt. Where, the second tailing component was produced after the second attrition step. It was composed of broken sand fragment remains weighing about 2.13% (see **Figure 9**).

Attrition scrubbing is an indispensable technology in silica sand processing programs to meet specifications of glass-making industries. When the attrition machine enters the processing flowsheet, the strong particle-particle friction forces between sand grains, from one side, and under strong turbulence inside the attrition tank, from the other side, an effective grain-grain rubbing or abrasion action occurs. This leads to the break down of adhered clayey coatings and ferruginous staining from the sand grain surfaces, subsequently, a grade improving in the silica sand sample takes place. Abrasion is characterized by the formation of fines and no noticeable change in the feed particle size distribution. Accordingly, attrition could be defined as the act of wearing by friction, and abrasion is a consequence of attrition. However, when the kinetic energy inside the attrition tank is high enough, chipping breakage, as a special case of cleavage is experienced, (see **Figure 10**). Then sharp edges on the sand surface can break off, (see **Figure 9**, yellow arrows) and weak location cracks in the sand body may show splitting, (see **Figure 9**, red arrows). In contrast to abrasion, chipping showed in general no fines formation, but on the other hand, it leaves behind broken silica fragments in different shapes and sizes as shown in **Figure 10**. In addition, notable change in the feed particle size distribution occurred (**Cleary and Morrison, 2016; Wahab et al., 2022; Abdullah, 2023; Ulusoy, 2023; Ravisankar et al., 2023; Othman et al., 2023; Benmebarek et al., 2023**).

XRF analyses results of sand fractions before and after attrition are illustrated in **Table 4**. The results showed that silica content increased from 90.10% in the attrition feed to 98.15% $SiO_2$ in the attrition product. On the other hand, iron oxide content decreased from 0.86% to

**Figure 7:** Classified sand sample showing an abundance of clayey coating on the grain surfaces


**Figure 8:** Classified head sample before (A) and after (B) attrition

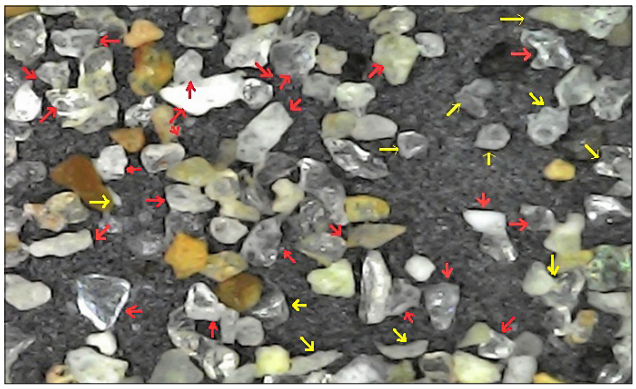

**Figure 9:** Broken sand fragments remain after the attrition process

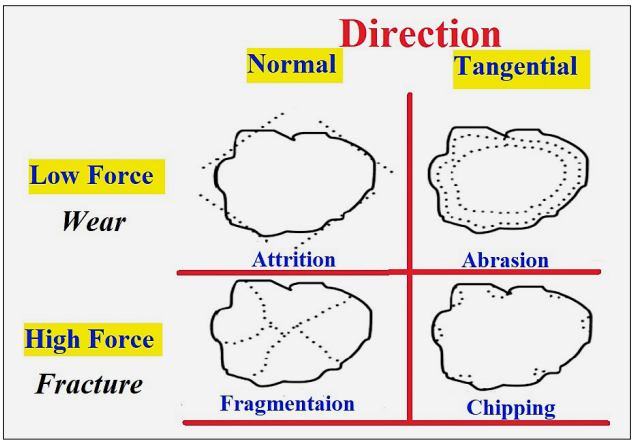


**Figure 10:** Influence of impact angle and impact force on particle grain (**Laarhoven et al., 2012; Cheong et al., 2003**)

reach 0.32% with removal reaching about 63%. In addition, alumina content decreased from 3.09% in the attrition feed to 0.64% $Al_2O_3$ in the attrition product with removal improvement reaching about 79%, as shown in **Table 4**.

On the other hand, **Table 5** illustrates the particle size distribution of sand samples before and after attrition. The results show notable changes throughout the sand

**Table 4:** XRF chemical analyses of different sand fractions before and after attrition

| Wt., % | Attrition feed, mesh | | | Attrition product, mesh | | |
|---|---|---|---|---|---|---|
| | 20/40 | 40/70 | 70/140 | 20/40 | 40/70 | 70/140 |
| $Na_2O$ | 0.726 | 1.260 | 1.60 | 0.431 | 0.780 | 0.970 |
| MgO | 0.371 | 0.595 | 1.057 | 0.131 | 0.150 | 0.181 |
| $Al_2O_3$ | 2.231 | 4.112 | 5.451 | 0.453 | 0.810 | 1.006 |
| $SiO_2$ | 93.102 | 87.35 | 80.11 | 98.18 | 96.70 | 93.51 |
| $P_2O_5$ | 0.331 | 0.416 | 0.459 | 0.027 | 0.037 | 0.075 |
| $SO_3$ | 0.709 | 0.601 | 2.357 | 0.035 | 0.057 | 0.046 |
| $K_2O$ | 0.430 | 0.814 | 0.851 | 0.353 | 0.627 | 0.74 |
| CaO | 1.211 | 2.332 | 4.292 | 0.240 | 0.601 | 1.216 |
| $TiO_2$ | 0.064 | 0.144 | 0.708 | 0.026 | 0.037 | 0.094 |
| MnO | --- | 0.024 | 0.059 | --- | --- | --- |
| $Fe_2O_3$ | 0.547 | 0.974 | 2.323 | 0.091 | 0.142 | 2.143 |
| SrO | 0.004 | 0.042 | 0.012 | 0.003 | 0.029 | 0.006 |
| $ZrO_2$ | 0.016 | 0.018 | 0.051 | 0.015 | 0.015 | 0.017 |
| Cl | 0.165 | 0.286 | 0.372 | 0.016 | 0.017 | --- |
| F | 0.093 | --- | --- | --- | --- | --- |
| ZnO | --- | --- | 0.051 | --- | --- | --- |

**Table 5:** Particle size distribution of sand samples before and after attrition

| Particle size | | Attrition feed | | | Attrition product | | |
|---|---|---|---|---|---|---|---|
| **Mesh** | **Microns** | **Wt., %** | **Wt., % Cum. Ret.** | **Wt. $_{total}$, %** | **Wt., %** | **Wt., % Cum. Ret.** | **Wt. $_{total,}$ %** |
| 20/30 | -850+600 | 37.86 | 37.86 | 61.99 | 27.80 | 27.80 | 53.20 |
| 30/35 | -600+500 | 14.52 | 52.38 | | 10.50 | 38.30 | |
| 35/40 | -500+425 | 9.61 | 61.99 | | 14.90 | 53.20 | |
| 40/45 | -425+355 | 9.72 | 71.71 | 26.77 | 9.40 | 62.60 | 36.50 |
| 45/50 | -355+300 | 8.36 | 80.07 | | 13.80 | 76.40 | |
| 50/60 | -300+250 | 5.72 | 85.79 | | 10.50 | 86.90 | |
| 60/70 | -250+212 | 2.97 | 88.76 | | 2.80 | 89.70 | |
| 70/100 | -212+150 | 5.95 | 94.71 | 11.24 | 5.90 | 95.60 | 10.30 |
| 100/120 | -150+125 | 3. 50 | 98.21 | | 3.10 | 98.70 | |
| 120/140 | 125+106 | 1.79 | 100.00 | | 1.30 | 100.00 | |

sample particle size distribution before and after attrition. Coarse sand particles between 850 microns to 500 microns showed a decrease in weight % reached 14.08%. In addition, sand particle size 500-425 microns increased after attrition from 9.61% to 14.90%, as shown in **Table 5**. On the other hand, particle sand size weight % between 355 microns to 250 microns increased from 14.08% to 24.30% with wt., the % difference reached 10.22%. Meanwhile, particles sized below 250 microns showed limited changes in their wt., %'s before and after attrition, as shown in **Table 5**. These results indicate that the attrition process strongly affected the coarse particles between 850 microns to 500 microns (see **Figure 11** and **Figure 12**).

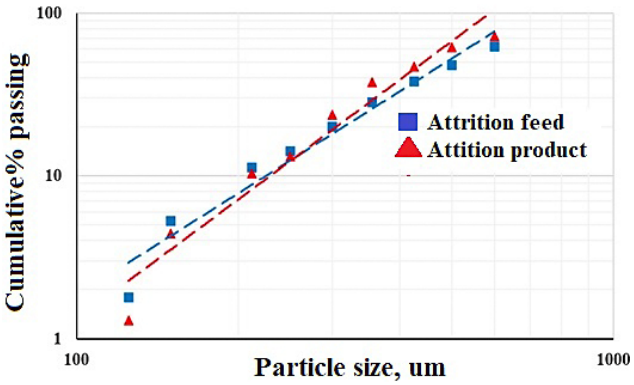


**Figure 11:** Cumulative passing wt., % vs particle size in sand attrition feed and attrition product

The attrition process of silica sand in general could be enhanced by adding a suitable amount of an environmentally friendly and inexpensive mixture of acids. Raising slurry temperature and reducing solid density to about 50% may also be required. This step could be attained in the last stage of the three stages attrition scrubbing operation. This additional stage could play a role in removing the remaining kaolinite and iron contaminants still present inside the cracks on the surfaces of some sand grains. It could be able also to clean sand grains surface from colored stains and splashes present on the grain surfaces. However, the purity of silica sand is not simply related to the content of impurity elements in the

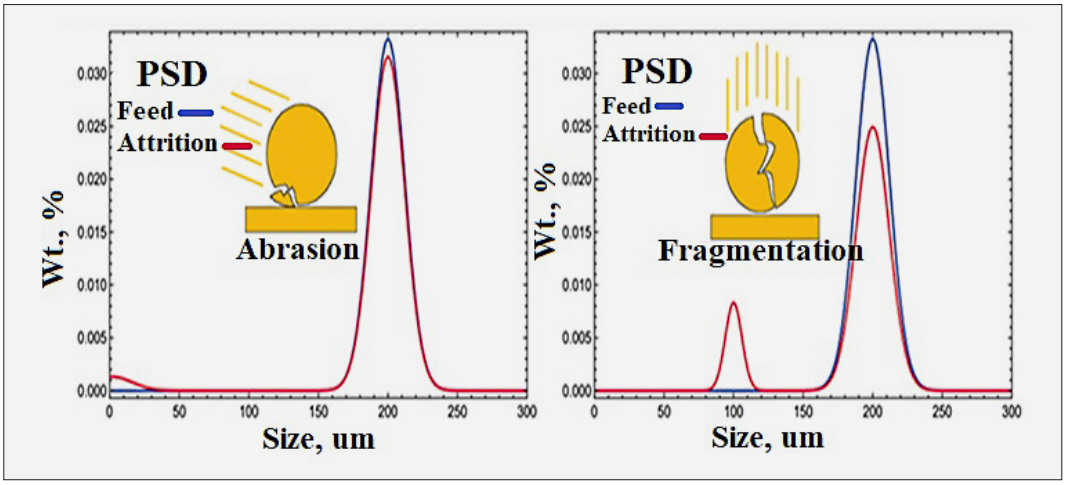


**Figure 12:** Different attrition actions on sand grains and its effect on the particle size distribution of attrition product

raw material but is closely related to the selectivity of impurities determined by the mineralogy study of the head sample. Therefore, basic research on silica sand mineralogy should be strengthened to identify the content, occurrence state, and distribution characteristics of impurity elements in the sand sample (**Guo et al., 2019; Kong et al., 2019; Ibrahim et al., 2022; Liu et al., 2023; Othman et al., 2024; Febriana et al., 2024**).

In a side study, the well dried attrition sand product was subjected as three sand sizes 850-425, 425-250, and 250-106 microns to magnetic separation using an "Eriez" Rare Earth Magna Roll dry high gradient separator (**Ibrahim et al., 2015**). The results showed that the three sand fractions contained magnetic residues in weight percentages of 0.72%, 1.42%, and 2.0%, respectively, meaning a weight percentage of about 4.14% by weight for the overall feeding sample. Magnetic fractions appeared mainly as black grains mixed with some colored ones. They were defined as iron minerals, mainly magnetite and some magnetic refractories minerals. Since these sand sections were present as 53.20, 36.50, and 10.30% by weight, then it could be assumed that these magnetic impurities were distributed by weight in an approximate ratio of 1: 2.88: 14.38 between the three attrition sand sections, respectively. Therefore, it can be asserted that conducting magnetic separation operations for the attrition product will not have a significant impact on increasing the quality of this sand as a whole, as the main two coarse fractions 20/40 mesh and 40/70 mesh favorable for fracking representing 89.70% wt., contained only 21.25% of the total magnetic impurities of the overall attrition product.

Turbidity test results of sand fraction samples before and after attrition are illustrated in **Table 6**. The results showed that after attrition, great improvement in the turbidity measures was recorded as 4.97, 6.65, and 16.91 NTU's from 1100, 996, and 986 NTU's with improving ratios reached 99.61, 99.09 and 98.28%, respectively. These remarkably improved ratios in all sand size fractions showed how much the attrition process was very violent and with adequate abrasion action to clean sand grains from almost all the ferruginous clayey matter. However, these new turbidity levels after attrition made the sand samples acceptable for fracking application.

The results of acid solubility measures of different sand fractions before and after treatment are illustrated in **Table 7**. Before attrition, acid solubility tests recorded 2.37, 4.16, and 8.10% in the factions 20/40, 40/70, and 70/140 mesh's, respectively, with an overall value recording 3.47%. From these results, it was noticed that all the acid solubility levels of untreated sand fractions and their average overall levels as well, were not matching the international standard measures (reached 2%). On the other hand, acid solubility measures of attrition sand fractions recorded 0.38, 0.82, and 2.23's, respectively, with an overall value of 0.73%, as shown in **Table 7**. It is obvious that all acid solubility levels of attrition sand fractions were in accordance with the acid solubility standard measures.

Bulk density measures the values of sand samples before and after attrition, as depicted in **Table 8**. After attrition, the bulk density measures of all sand fractions showed an increase. This increase in bulk density values in different sand size fractions is often the result of an increase in its chemical grade after attrition, and other physical properties that follow, which led to an improvement in its bulk density measurements. The proppants' typical bulk density (BD) is between 1.60 and 2.00 g/cm³. Bulk density is an important physical property for frac sand raw materials. It describes the mass of proppant that fills a unit volume and includes both proppant and porosity. It is used to determine the mass of a proppant required to fill a fracture of layers containing oil/gas. Meanwhile, apparent density is measured with a

**Table 6:** Turbidity measure results

| Sand sample | Particle size, mesh | Turbidity, NTU |
|---|---|---|
| Feed samples | 20/40 | 1100 |
| | 40/70 | 996 |
| | 70/140 | 986 |
| Calc. total | | 1050 |
| Attrition products | 20/40 | 4.97 |
| | 40/70 | 6.65 |
| | 70/140 | 16.91 |
| Calc. total | | 6.813 |
| Fracking limit | | ≤250 |

**Table 7:** Acid solubility results

| Product | Size (mesh) | Original wt., g | Wt., after solubility, g. | Acid solubility, % | Fracking limit |
|---|---|---|---|---|---|
| Feeding samples | 20/40 | 5.05 | 4.9303 | 2.37 | 2 |
| | 40/70 | 5.018 | 4.8123 | 4.10 | 3 |
| | 70/140 | 5.077 | 4.6658 | 8.10 | 3 |
| Calc. total | | | | 3.48 | |
| Attrition products | 20/40 | 5.0246 | 5.0053 | 0.38 | 2 |
| | 40/70 | 5.0543 | 5.0129 | 0.82 | 3 |
| | 70/140 | 5.012 | 4.9002 | 2.23 | 3 |
| Calc. total | | | | 0.73 | |

**Table 8:** Bulk density measures of original and attrition samples

| Sample | Particle size, mesh | Bulk density, g/cc |
|---|---|---|
| Original sand | 20/40 | 1.594 |
| | 40/70 | 1.524 |
| | 70/140 | 1.180 |
| | Calc. total1. | 1605 |
| Attrition sand | 20/40 | 1.652 |
| | 40/70 | 1.583 |
| | 70/140 | 1.498 |
| | Calc. total | 1.611 |
| For Fracking | 1.60-2.00 g/cc | |

low-viscosity fluid (like toluene) that wets the particle surface and includes the pore space inaccessible to the fluid. On the other hand, the absolute density excludes pores that can be in the proppant as well as void spaces between the proppant particles (**American National Standards Institute B74.4 1992; Gaber et al, 2021**). The bulk density of sand samples was obtained according to API 19C recommended standard. A 100 ml measuring cylinder was placed on a weighing balance unit and set to a zero reading. Sand samples were slowly and carefully poured into the measuring cylinder until the 100 ml mark. The reading on the weighing balance unit was recorded and the bulk density was calculated as:

$$\text{Bulk density (g/cc)} = \text{Mass of dry sand sample (g)} / \text{ / volume of dry sand sample (cc)} \quad (1)$$

Higher bulk density proppant grains are of higher strength, have more resistivity to crushing, and more durability, which is desirable for the fracking industry. The importance of measuring bulk density comes from its connection with the proppant porosity and hence its resistance, which is one of the main properties to be considered since it defines the lifetime and the limit of closure stress. Viscosity and density are two different physical parameters that are not directly related. They are indirectly related through temperature. In general, for any fluids, when the temperature is increased, its density decreases and fluid becomes less viscous. The increase of fluid viscosity leads to an increase of flow resistance of the clean fracturing fluid, the limitation of fracture propagation, and the small damage variable (**de Campos et al., 2018**; **Wahab et al., 2022**).

### 3.2.2. Improved particle size distribution

Particle size distribution results of sand samples showed that 20/40 mesh sand represented 61.99% and 53.20% before and after attrition, whereas the 20/70 mesh sand fraction represented 88.76% and 89.70% before and after attrition (see **Figure 13**). These results showed that the sand sample has reasonable narrow particle size distribution, which is preferable for the fracking industry. Hence it retains a high permeability and provides fractures with the highest conductivity (**Liang et al., 2016; Liang et al., 2020; Lui et al., 2021**).

Hydraulic fracturing, or "fracking," is an oil and gas well development process that typically involves injecting water, sand (or other proppants), and chemicals under high pressure into a bedrock formation via the well. The aim of this process is to create new fractures in the rock, as well as increase the size, extent, and connectivity of existing fractures. The task of the proppants in the fracking fluid is to keep the fissures in the rock open and in accordance to maintain the permeability to oil and gas. For good permeability, proppant particle size must be well matched to the size of the cracks and the size distribution must be narrow (**US Geological Survey, 2024**).

**Frac sand is named by the size of the grains.** The coarsest grains standard for frac sand is 20/40. This means that 90 percent of the sand is fine enough to pass through a 20-mesh sieve and is coarse enough to be retained on a 40-mesh sieve. As long as the sand sample meets these requirements, then it is called a 20/40 frac sand sample. Some other common standard sizes are 30/50, 40/70, and 50/140 also referred to as "100 mesh." Particle Size Distribution refers to the range of sizes of particles present in a sample, which is crucial in various manufacturing processes. When a material has a narrow particle distribution, this means all the particles within the material have a similar size. The particles are more or less uniform, and the term "narrow particle distribu-

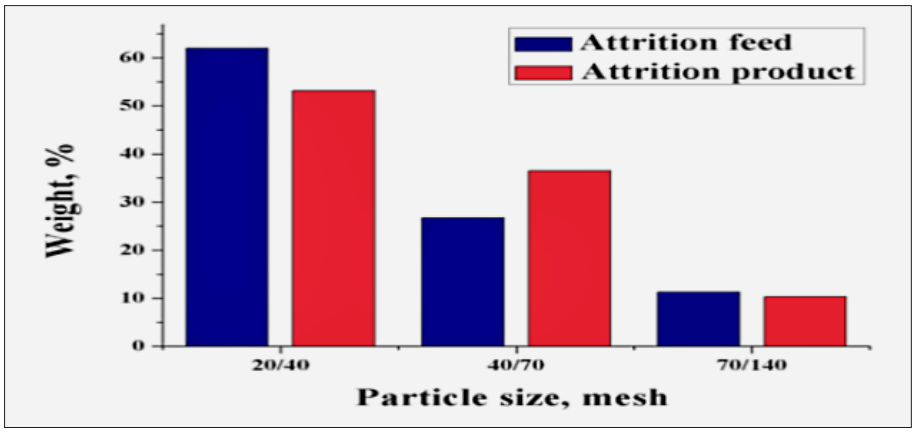


**Figure 13:** Different sand fractions wt., % before and after attrition

tion" is often used to describe this uniformity. However, determining the best size distribution of particles depends upon what the material is and how it's being used. Additionally, the uniformity of these particles will determine how a material will react under various conditions. Analyzing particle size distribution helps ensure products function as they should, and aids the investigation of a material's properties, including its strength or how the material reacts to chemicals (**Liang et al., 2016; Liang et al., 2020; Lui et al., 2021**).

### 3.2.3. Improved mechanical and rheological characteristics

The crush resistance results of sand fractions samples before and after attrition are shown in **Table 9**. The results indicate that crush resistance of all sand size fraction samples were of acceptable values for fracking application. However, the crushability measures after attrition showed improvement from 8.15% to 6.19% by a ratio of 24.05% (see **Figure 14**). This improvement was a result of the efficient attrition process, either through abrasion and/or fragmentation- chipping mechanisms. An efficient attrition process means that sand grains were cleaned from most fines that may cause the blocking of well openings, from one side, and from the weak sand particles that showed splitting and may cause proppant embedment destruction, from the other side. Injecting proppants into oil and gas fractures tends to maintain conductivity by keeping them open. So that smooth flow of proppant fluids into the wellbore is ensured, hence, proppants are required to possess sufficient strength to sustain the closure pressures acting upon them. Propped fracture conductivity is affected by processes such as the crushing of proppants, the creation of fines and proppant embedment. The process of proppant crushing and embedment are then aggravated by the properties of the reservoir, fracturing fluid and the proppants (**Zheng and Tannant, 2016; Hari et al., 2021, Sanchez et al., 2022**).

**Table 9:** Crush resistance % measures of sand samples before and after attrition

| Sand product | Particle size (mesh) | Sample wt., g | Under size, g. | Crush resistance, % |
|---|---|---|---|---|
| Before attrition | 20/40 | 39.37 | 3.76 | 9.55 |
| | 40/70 | 37.64 | 2.39 | 6.35 |
| | 70/140 | 29.15 | 1.37 | 4.70 |
| Total | | | | 8.15 |
| After attrition | 20/40 | 40.80 | 3.06 | 7.50 |
| | 40/70 | 39.10 | 2.10 | 5.37 |
| | 70/140 | 37.00 | 0.86 | 2.32 |
| Total | | | | 6.19 |
| Fracking limit | | | | ≤10 |

Sphericity and roundness measures of different sand fractions before and after attrition (see **Figure 15** and **Figure 16**) compared with a Krumbein and Sloss chart (see **Figure 17**), are shown in **Table 10** and **Table 11**. On the other hand, sphericity and roundness measures of sand fractions before and after attrition (see **Figure 18**, **Figure 19**, and **Figure 20**) after the numerical method based on the computational geometry of two-dimensional images of sand particles using a Mega Pixels microscope are shown in **Table 12** and **Table 13**. Sphericity and roundness measures after the first technique recorded 0.626 and 0.631 for the sand sample before attrition. After attrition, they recorded 0.748 and 0.735, respectively, as shown in **Table 10** and **Table 11**. On the other hand, sphericity and roundness measures after the second technique recorded 0.747 and 0.71, respectively for the sand sample after attrition, as shown in **Table 12** and **Table 13**. It is remarked that the measuring technique using a Wild Heerbrugg M3 stereo microscope and that using the Krumbein and Sloss chart, from one side, and by using computational geometry of two-dimensional images using a Mega Pixels microscope, from the other side, are almost near to each other.

The results showed that all the sphericity and roundness measure values for the sand sample before and after attrition were within the permissible range of hydraulic fracturing applications according to International Standards. In addition, the sphericity and roundness measure results after attrition showed improvement by ratios

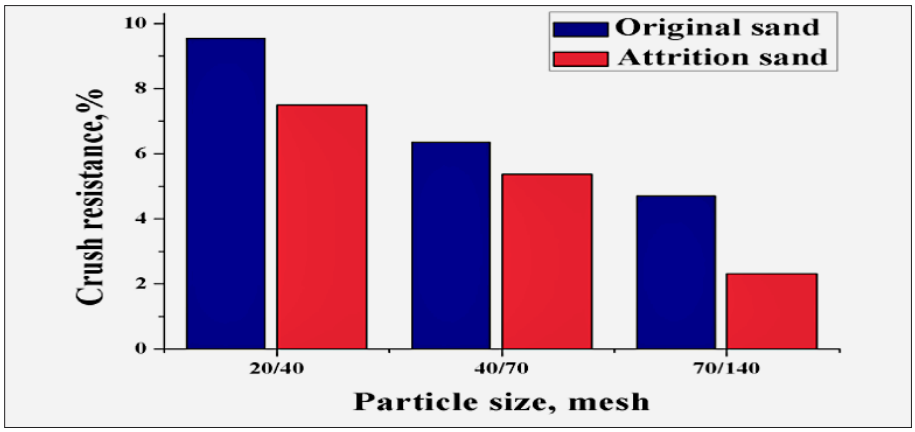


**Figure 14:** Crush resistance measures

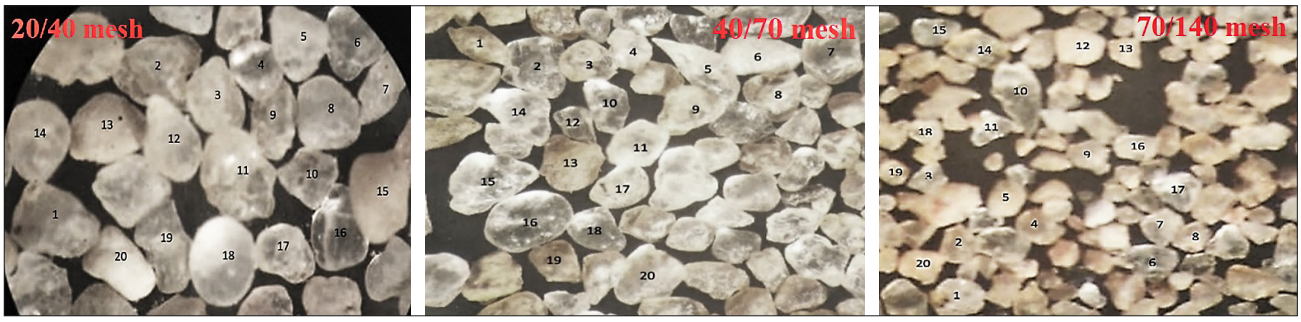


**Figure 15:** Sphericity and roundness calculations of sand fractions before attrition

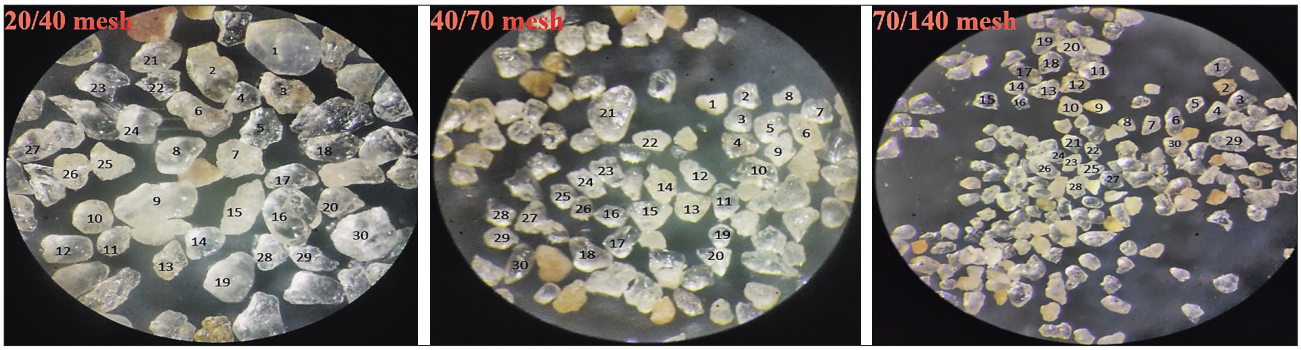


**Figure 16:** Sphericity and roundness calculations of sand fractions after attrition

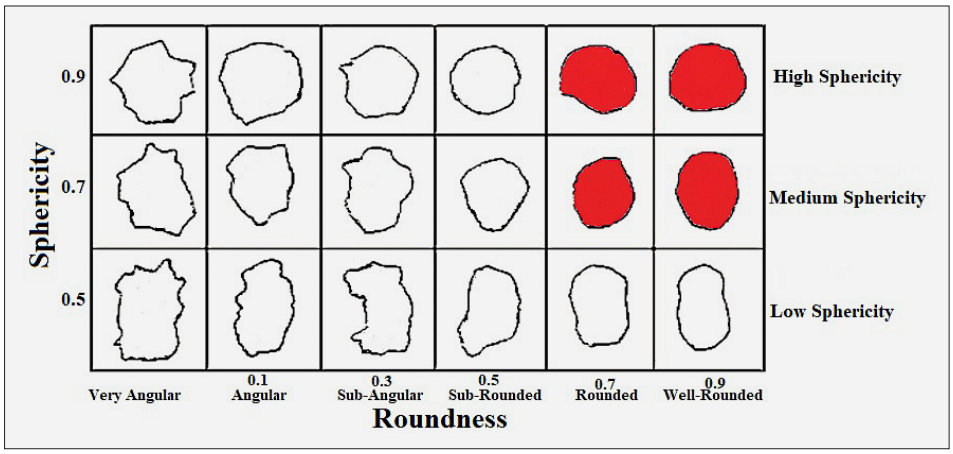


**Figure 17:** "Krumbein and Sloss" Chart (**Krumbein and Sloss, 1963**)

reaching 19.11% and 16.72%, respectively (see **Figure 21** and **Figure 22**). The results showed that after attrition, the improvement in the sphericity measures for sand fractions 20/40, 40/70, and 70/140 mesh reached 23.61%, 15.47%, and 12.35%, respectively. On the other hand, the improvement in the roundness measures for sand fractions 20/40, 40/70, and 70/140 mesh after attrition reached 14.39%, 24.48%, and 16.38%, respectively. It can be noticed that the highest improvement value in sphericity measures was at the size fraction 20/40 mesh, reaching 23.61%, as depicted in **Table 12**. Where the highest improvement value in roundness measures was at the size fraction 40/70, reaching 24.48%, as shown in **Table 13**. These improvement ratios were of almost equal values. From these results, it seemed that there was a consistency in trends which could be remarked between the change in the particle size distribution of attrition products, especially in the grain sizes 20/30 and 30/35 mesh's (main weight% loser fractions) and in the size fractions 35/40, 45/50, and 50/60 mesh's (main weight% gainer fractions) from one side, and between the improvement in their crushability resistance, sphericity and roundness measures on the other side. This means that the coarse sand grains in sizes 20/30 and 30/35 mesh's were relatively the weaker grains in the sand sample and they were the ones that witnessed the largest share of the splitting and fragmentation processes during the attrition process. Therefore, there was an improvement in their crushability and sphericity measures after attrition.

At the same time, the smaller grain sizes, especially in 35/40, 45/50, and 50/60 mesh's fractions, showed an in-

**Table 10:** Sphericity and roundness measures of sand fractions before attrition

| Grain no. | Sphericity | | | Roundness | | |
|---|---|---|---|---|---|---|
| | 20/40 | 40/70 | 70/140 | 20/40 | 40/70 | 70/140 |
| 1 | 0.7 | 0.5 | 0.7 | 0.7 | 0.5 | 0.7 |
| 2 | 0.7 | 0.9 | 0.5 | 0.5 | 0.5 | 0.7 |
| 3 | 0.7 | 0.9 | 0.7 | 0.7 | 0.7 | 0.5 |
| 4 | 0.7 | 0.7 | 0.7 | 0.9 | 0.5 | 0.7 |
| 5 | 0.7 | 0.5 | 0.7 | 0.7 | 0.5 | 0.7 |
| 6 | 0.7 | 0.7 | 0.7 | 0.5 | 0.5 | 0.7 |
| 7 | 0.5 | 0.9 | 0.7 | 0.3 | 0.7 | 0.7 |
| 8 | 0.7 | 0.9 | 0.7 | 0.7 | 0.7 | 0.7 |
| 9 | 0.5 | 0.7 | 0.7 | 0.5 | 0.7 | 0.5 |
| 10 | 0.7 | 0.5 | 0.3 | 0.5 | 0.5 | 0.5 |
| 11 | 0.7 | 0.9 | 0.5 | 0.5 | 0.5 | 0.7 |
| 12 | 0.5 | 0.7 | 0.9 | 0.7 | 0.5 | 0.7 |
| 13 | 0.7 | 0.9 | 0.7 | 0.7 | 0.5 | 0.3 |
| 14 | 0.5 | 0.7 | 0.7 | 0.9 | 0.5 | 0.5 |
| 15 | 0.5 | 0.7 | 0.7 | 0.7 | 0.5 | 0.7 |
| 16 | 0.7 | 0.9 | 0.7 | 0.7 | 0.9 | 0.7 |
| 17 | 0.5 | 0.7 | 0.9 | 0.9 | 0.7 | 0.7 |
| 18 | 0.5 | 0.9 | 0.5 | 0.9 | 0.7 | 0.7 |
| 19 | 0.5 | 0.7 | 0.9 | 0.5 | 0.5 | 0.7 |
| 20 | 0.5 | 0.9 | 0.7 | 0.7 | 0.5 | 0.5 |
| Sum | 12.2 | 15.2 | 13.6 | 13.2 | 11.6 | 12.6 |
| Mean | 0.61 | 0.64 | 0.68 | 0.66 | 0.58 | 0.63 |
| Total | 0.626 | | | 0.631 | | |

**Table 11:** Sphericity and roundness measures of sand fractions after attrition

| Grain No. | Sphericity | | | Roundness | | |
|---|---|---|---|---|---|---|
| | 20/40 | 40/70 | 70/140 | 20/40 | 40/70 | 70/140 |
| 1 | 0.88 | 0.78 | 0.88 | 0.94 | 0.81 | 0.71 |
| 2 | 0.72 | 0.57 | 0.70 | 0.65 | 0.66 | 0.58 |
| 3 | 0.51 | 0.77 | 0.95 | 0.84 | 0.47 | 0.72 |
| 4 | 0.56 | 0.86 | 0.63 | 0.60 | 0.77 | 0.72 |
| 5 | 0.80 | 0.74 | 0.72 | 0.60 | 0.87 | 0.66 |
| 6 | 0.74 | 0.70 | 0.66 | 0.68 | 0.63 | 0.63 |
| 7 | 0.59 | 0.73 | 0.55 | 0.83 | 0.92 | 0.63 |
| 8 | 0.73 | 0.74 | 0.46 | 0.88 | 0.67 | 0.66 |
| 9 | 0.98 | 0.62 | 0.87 | 0.97 | 0.66 | 0.76 |
| 10 | 0.65 | 0.71 | 0.96 | 0.87 | 0.49 | 0.66 |
| 11 | 0.96 | 0.74 | 0.54 | 0.37 | 0.76 | 0.61 |
| 12 | 0.80 | 0.67 | 0.77 | 0.64 | 0.75 | 0.77 |
| 13 | 0.52 | 0.81 | 0.86 | 0.68 | 0.71 | 0.71 |
| 14 | 0.80 | 0.62 | 0.96 | 0.87 | 0.75 | 0.83 |
| 15 | 0.54 | 0.79 | 0.55 | 0.69 | 0.71 | 0.68 |
| 16 | 0.74 | 0.98 | 0.78 | 0.75 | 0.72 | 0.69 |
| 17 | 0.80 | 0.67 | 0.85 | 0.87 | 0.80 | 0.74 |
| 18 | 0.74 | 0.79 | 0.92 | 0.49 | 0.70 | 0.54 |
| 19 | 0.97 | 0.93 | 0.95 | 0.90 | 0.81 | 0.61 |
| 20 | 0.97 | 0.56 | 0.72 | 0.90 | 0.79 | 0.59 |
| Sum | 15.00 | 14.78 | 15.28 | 15.02 | 14.45 | 13.50 |
| Mean | 0.75 | 0.74 | 0.76 | 0.75 | 0.72 | 0.67 |
| Total | 0.748 | | | 0.735 | | |

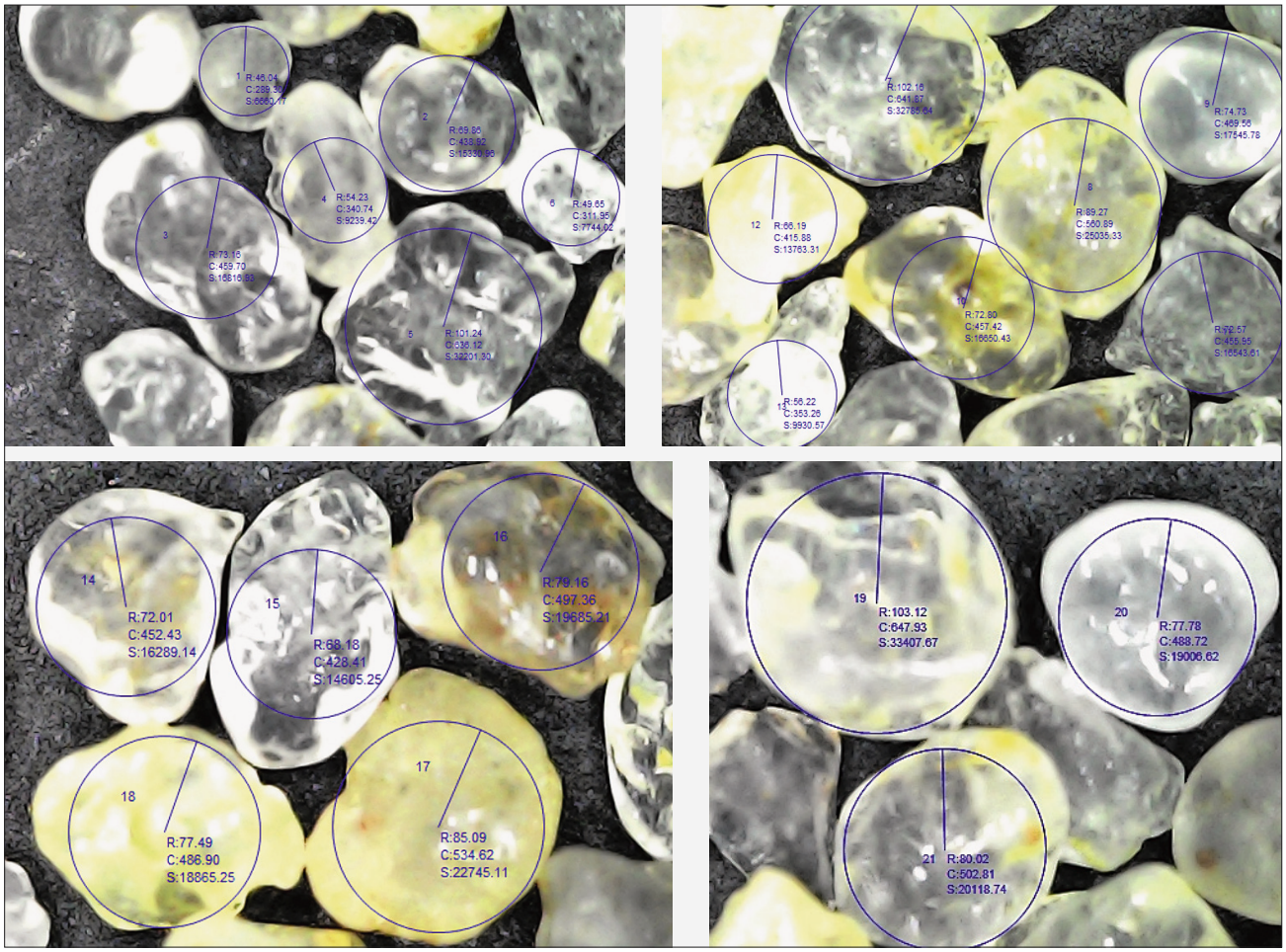


**Figure 18:** Sphericity and roundness measures of 20/40 mesh attrition sand product

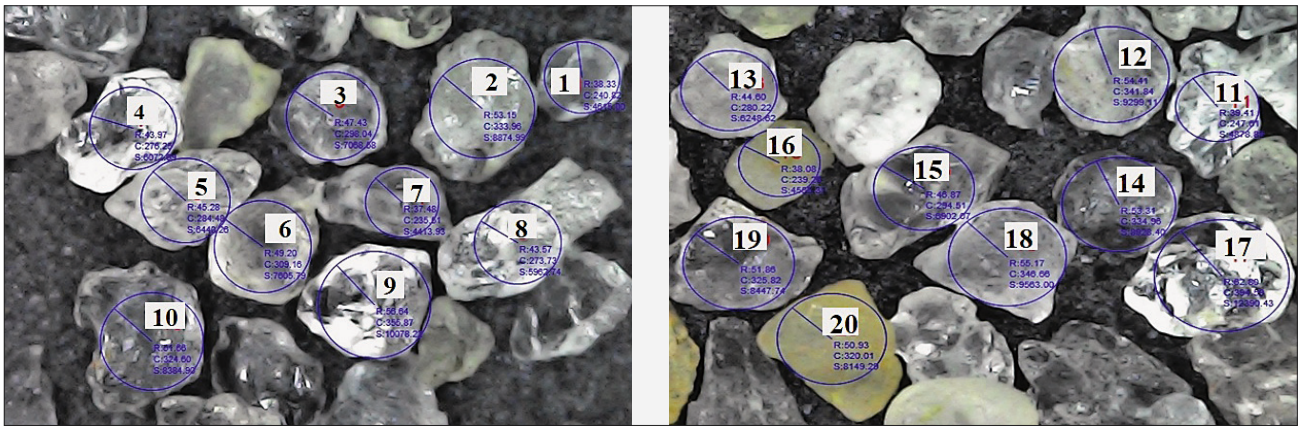

**Figure 19:** Sphericity and roundness measures of 40/70 mesh attrition sand product

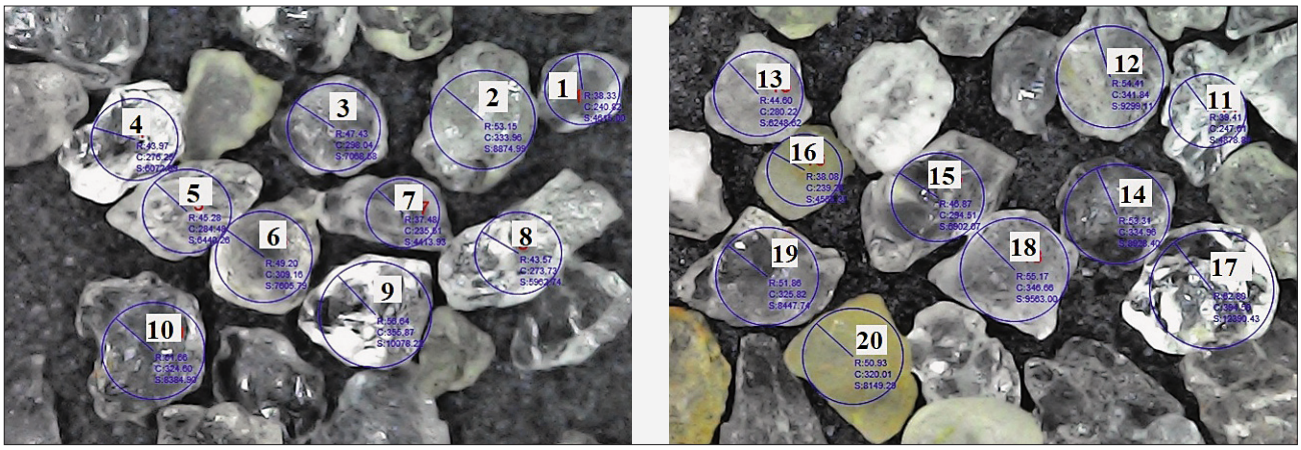

**Figure 20:** Sphericity and roundness measures of 70/140 mesh attrition sand fraction

**Table 12:** Sphericity and roundness of 20/40 mesh sand fraction after attrition

| Grain No. | R | R1 | Roundness | Nominal diameter | Maximum intercept | Sphericity |
|---|---|---|---|---|---|---|
| 1 | 46.04 | 43.57 | 0.94 | 98 | 111 | 0.88 |
| 2 | 69.86 | 42.3 | 0.65 | 143 | 196 | 0.72 |
| 3 | 73.16 | 50.2 | 0.84 | 147 | 283 | 0.51 |
| 4 | 54.23 | 19.12 | 0.60 | 124 | 220 | 0.56 |
| 5 | 101.24 | 37.18 | 0.60 | 205 | 254 | 0.80 |
| 6 | 49.65 | 32.8 | 0.68 | 100 | 134 | 0.74 |
| 7 | 102.16 | 59.12 | 0.83 | 159 | 269 | 0.59 |
| 8 | 89.27 | 85.2 | 0.88 | 190 | 259.7 | 0.73 |
| 9 | 74.73 | 72.5 | 0.97 | 160 | 163 | 0.98 |
| 10 | 72.8 | 70 | 0.87 | 152 | 232 | 0.65 |
| 11 | 72.57 | 12.81 | 0.37 | 157 | 162 | 0.96 |
| 12 | 66.19 | 29.15 | 0.64 | 149 | 185 | 0.80 |
| 13 | 56.22 | 33.29 | 0.68 | 113 | 214 | 0.52 |
| 14 | 72.01 | 48.17 | 0.87 | 153 | 190.7 | 0.80 |
| 15 | 68.18 | 61 | 0.69 | 135 | 250 | 0.54 |
| 16 | 79.16 | 43.82 | 0.75 | 163.7 | 219 | 0.74 |
| 17 | 85.09 | 60.7 | 0.87 | 167.16 | 207.34 | 0.80 |
| 18 | 77.49 | 57.5 | 0.49 | 162.5 | 219.02 | 0.74 |
| 19 | 103.12 | 93.2 | 0.90 | 225 | 230 | 0.97 |
| 20 | 77.7 | 74 | 0.90 | 177 | 182 | 0.97 |
| 21 | 80.02 | 73 | 0.84 | 172 | 204 | 0.84 |
| Calc. mean average | 0.712 | | | 0.75 | | |

**Table 13:** Sphericity and roundness of 40/70 mesh sand fraction after attrition

| Grain No. | R | R1 | Roundness | Nominal diameter | Maximum intercept | Sphericity |
|---|---|---|---|---|---|---|
| 1 | 45.35 | 38.21 | 0.81 | 93.7 | 119.82 | 0.78 |
| 2 | 28.20 | 13.06 | 0.66 | 50.22 | 87.7 | 0.57 |
| 3 | 41.48 | 14.42 | 0.47 | 99.27 | 128.14 | 0.77 |
| 4 | 28.02 | 18.44 | 0.77 | 59.03 | 68.07 | 0.86 |
| 5 | 23.54 | 18.1 | 0.87 | 51.11 | 69.12 | 0.74 |
| 6 | 33.7 | 18.0 | 0.63 | 68.88 | 98.25 | 0.70 |
| 7 | 33.29 | 28.18 | 0.92 | 66.57 | 90.68 | 0.73 |
| 8 | 35.78 | 10.44 | 0.67 | 73.05 | 98.46 | 0.74 |
| 9 | 42.15 | 32.06 | 0.66 | 81.10 | 130.4 | 0.62 |
| 10 | 32.89 | 10.32 | 0.49 | 65.20 | 91.55 | 0.71 |
| 11 | 50.22 | 27.6 | 0.76 | 103.6 | 140.2 | 0.74 |
| 12 | 35.11 | 24.33 | 0.75 | 75.29 | 112.2 | 0.67 |
| 13 | 34.06 | 20.56 | 0.71 | 76.10 | 93.96 | 0.81 |
| 14 | 57.04 | 39.3 | 0.75 | 113.11 | 181.01 | 0.62 |
| 15 | 36.83 | 13.42 | 0.71 | 76.22 | 95.88 | 0.79 |
| 16 | 51.31 | 42.00 | 0.72 | 117.00 | 119.00 | 0.98 |
| 17 | 44.41 | 33.62 | 0.80 | 82.7 | 122.43 | 0.67 |
| 18 | 28.2 | 14.76 | 0.70 | 68.01 | 85.43 | 0.79 |
| 19 | 41.01 | 30.00 | 0.81 | 87.32 | 94.07 | 0.93 |
| 20 | 28.06 | 14.04 | 0.79 | 58.6 | 104.69 | 0.56 |
| 21 | 38.01 | 20.62 | 0.71 | 78.4 | 103.25 | 0.75 |
| Calc mean average | 0.72 | | | 0.74 | | |

**Table 14:** Sphericity and roundness results of 70/140 mesh sand fraction after attrition

| Grain No. | R | R1 | Roundness | Nominal diameter | Maximum intercept | Sphericity |
|---|---|---|---|---|---|---|
| 1 | 38.33 | 18.44 | 0.71 | 90.60 | 102.65 | 0.88 |
| 2 | 53.15 | 22.14 | 0.58 | 113.00 | 160.83 | 0.70 |
| 3 | 47.43 | 23.71 | 0.72 | 104.62 | 110.00 | 0.95 |
| 4 | 43.97 | 23.19 | 0.72 | 95.20 | 151.33 | 0.63 |
| 5 | 45.28 | 25.96 | 0.66 | 103.32 | 144.00 | 0.72 |
| 6 | 49.20 | 16.23 | 0.63 | 98.29 | 149.00 | 0.66 |
| 7 | 37.48 | 16.25 | 0.63 | 78.09 | 140.50 | 0.55 |
| 8 | 43.57 | 21.00 | 0.66 | 93.00 | 199.00 | 0.46 |
| 9 | 56.64 | 39.24 | 0.76 | 121.50 | 139.20 | 0.87 |
| 10 | 51.66 | 18.60 | 0.66 | 153.60 | 159.00 | 0.96 |
| 11 | 39.41 | 17.10 | 0.61 | 82.00 | 152.00 | 0.54 |
| 12 | 54.41 | 30.41 | 0.77 | 115.00 | 148.00 | 0.77 |
| 13 | 44.6 | 21.10 | 0.71 | 98.00 | 114.00 | 0.86 |
| 14 | 53.31 | 33.42 | 0.83 | 114.28 | 119.00 | 0.96 |
| 15 | 46.87 | 26.17 | 0.68 | 97.00 | 174.00 | 0.55 |
| 16 | 38.06 | 25.06 | 0.69 | 78.00 | 99.00 | 0.78 |
| 17 | 62.80 | 41.11 | 0.74 | 137.00 | 160.50 | 0.85 |
| 18 | 55.17 | 23.40 | 0.54 | 110.08 | 119.89 | 0.92 |
| 19 | 51.86 | 27.02 | 0.61 | 122.00 | 127.63 | 0.95 |
| 20 | 50.93 | 28.16 | 0.59 | 106.12 | 146.20 | 0.72 |
| Calc. mean average | | 0.65 | | 0.76 | | |

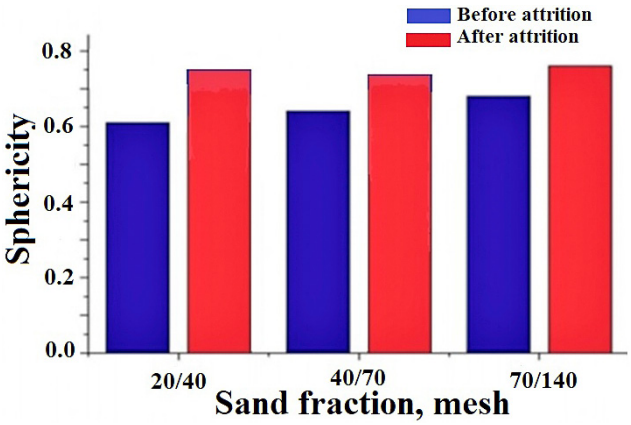


**Figure 21:** Sphericity measures of sand fractions before and after attrition

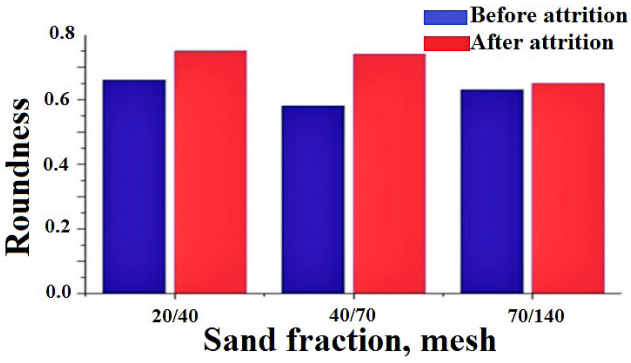


**Figure 22:** Roundness measures of sand fractions before and after attrition

crease in their weight % as they were the ones that received the majority of the split sand grains after coarser fractions. In accordance, they showed better mechanical and grain shape properties, that allow them to have the ability to withstand pressure without breaking and to pack them tightly together and hold open the fractures in the rock, maximizing the flow of oil and gas.

## 4. Conclusions

A one-ton technological silica sand ore sample belonging to the "Egypt's Future Quarries" Company, south west Cairo, was investigated for hydraulic fracking industry purposes. Preliminary physical tests of the sample showed encouraging results. Yet, its grade quality was unacceptable as a proppant according to the International Organization for Standardization. A simple beneficiation flowsheet was suggested. It included sieve classification and attrition scrubbing using a 50-liter capacity "Denver" machine at severe agitation speeds and pulp density conditions for 15 minutes.

The results showed that the most substantial improvement in silica grade was achieved early in the first five minutes of the attrition process. This was attained with the removal of most of the ferruginous clayey matter from the sand grains' surface. Where the greatest increase in $SiO_2$ content (from 90.10% to 98.15% $SiO_2$), and the greatest decrease in $Al_2O_3$ and $Fe_2O_3$ content (from 3.09% and 0.86% to 0.64% and 0.32%, respectively) were achieved. This grade improvement was reflected in the remarkable decrease in turbidity% measures from 1059 NTU in the attrition feed to 6.813 NTU in the attrition product with improvement reaching 99.35%. This improvement was also reflected in decreasing the acid solubility measures from 3.47% in the attrition feed to 0.73% in the attrition product with improvement reaching 78.97%. This improvement in turbidity and acid solubility measures transformed the sample from unacceptable for hydraulic fracking application to an acceptable sand sample according to the International Organization for Standardization.

On the other hand, microscopic investigation of the broken silica fragments residue, resulting after the second attrition stage, explained their presence as a result of trimming sharp edges and curves, as well as the breaking which occurred in the weak areas or cracks of some sand grains. Getting rid all of these residues showed an improvement in the mechanical and rheological measures of the attrition sand product. The crushability resistance, sphericity, and roundness measures after attrition were improved by ratios reaching 24.06%, 19.11%, and 16.72%, respectively. In addition, particle size distribution of the attrition product showed improvement to be narrower, which is desirable as a proppant for the hydraulic fracking industry.

**Nomenclature List:**

International Organization for Standardization: IOS

American Petroleum Institute: API

Lonquist Engineering Company: LLC

Formazin/Nephelometric Turbidity Unit: FTU/NTU

Rare Earth Roll: RER

X-ray fluorescence analysis: XRF

X-ray diffractometry analysis: XRD

Hydrochloric acid/ Hydrofluoric acid solution: HCl/ HF solution

A megapascal, is a unit of pressure: MPa

Pound per square inch, is the pressure that results when a 1-pound force is applied to a unit area of 1 square inch: PSI

## 5. References

Abdel Kader, A. K., Kordík, P., Khalil, A., Mekkawi, M., El-Bohoty, M. (2013): Interpretation of Geophysical Data at EL Fayoum – Dahshour Area, Egypt Using Three Dimensional Models. Arabian Journal for Science and Engineering 38, 7, 1769–1784. https://doi.org/10.1007/s13369-012-0385-0

Abdullah, W. R. (2020): Standard Sand Specifications Development by Mechanical Attrition Scrubbing to Make it Convenient for the Cement Industry. Key Engineering Ma-

terials 870, 61-70. https://doi.org/10.4028/www.scientific.net/KEM.870.61

Abdullah, W. R. (2023): Improving Silica Sand Specifications for Making Colourless Glasses by Using Chemical and Physical Methods. Solid State Phenomena 341. Materials Science and Engineering. https://doi.org/10.4028/p-n97lx4.

American Petroleum Institute (API 19C) (2008): Recommended Practice for Measurement of Proppants Used in Hydraulic Fracturing and Gravel-packing Operations, First Edition. Washington, DC: API.

Arslan, V. (2021): Modelling and Optimization of Iron Removal from Silica Sand Under Ultrasound-Assisted Leaching by Response Surface Methodology. Mining, Metallurgy & Exploration 38, 2229–37. https://doi.org/10.1007/s42461-021-00457-0

Assem, A.I. and Nasr-El-Din, H.A. (2015): Interactions Between Mud Acid and Sand Proppants. SPE North Africa Technical Conference and Exhibition, Cairo, Egypt, September 2015. Paper Number: SPE-175833-MS. https://doi.org/10.2118/175833-MS

Benmebarek, M., Rad, M. and Benmebarek, S. (2023): 3D DEM Analysis of Particle Breakage Effect on Direct Shear Tests of Coarse Sand. Materials 16, 5025. https://doi.org/10.3390/ma16145025

Cheong, Y.S., Salman, A.D., Hounslow, M.J. (2003): Effect of impact angle and velocity on the fragment size distribution of glass spheres. Powder Technology 138, 189–200. https://doi.org/10.1016/j.powtec.2003.09.010

Cleary, P. W. and Morrison, R. D. (2016): Comminution mechanisms, particle shape evolution and collision energy partitioning in tumbling mills. Minerals Engineering 86, 75–95. https://doi.org/10.1016/j. mineng.2015.12.006

de Campos, V. P. P., Sansone, E. C., e Silva1, G. F. B. L. (2018): Hydraulic fracturing proppants. Cerâmica 64, 219-229. Scientific Electronic Library Online, Brazil. http://dx.doi.org/10.1590/0366-69132018643702219

Fadl, A. and Abdou, M. (2019): Proppants categories for hydraulic fracturing process of petroleum wells: a review. Global Journal of Environmental Sciences 2, 1–2. https://doi.org/10.33552/ GJES.2019.000532

Febriana, E., Mayangsari, W., Prasetyo, A. B., Irawan, J., Sulistiyono, E., Handayani, M., Firdiyono, F. and Soedarsono, J. W. (2024): Reducing Impurities of Silica Sand by One Step and Two Step Leaching. 5th International Seminar on Metallurgy and Materials (ISMM2022) AIP Conf. Proc. 3003, 020112-1–020112-9. https://doi.org/10.1063/5.0186247

Frac Sand (Sand Proppant) & Resin Coated Sand, Investment Opportunity Scorecard. (2024): Mining & Metals.

Fuerstenau, M. C. and Han, K. N. (2003): Principles of Mineral Processing. SEM, Science- 573 pages. ISBN-13. 978-0873351676.

Fitzgerald, T. (2013): Frackonomics: Some economics of hydraulic fracturing. Case W. Res. L. Rev. 63, 1337. https://scholarlycommons.law.case.edu/caselrev/vol63/iss4/13.

Gaber, M. and Gamal El-Din, A. (2021): Characterization of some Egyptian white sand and dunes for utilization as hydraulic fracturing sand for tight oil well layers. Annals of the Geological Survey of Egypt 38. https://www.researchgate.net/publication/345947748.

Gu, M., Dao, E., Mohanty, K.K. (2015): Investigation of ultralight weight proppant application in shale fracturing. Fuel 150, 191-201. https://doi.org/10.1016/j.fuel.2015.02.019

Guo, W., Han, Y., Zhu, Y., Liu, Q. and Li, Y. (2019): Analysis of High-purity Quartz Sand Resources and Its Processing Technologies. Metal Mine 2, 22–28. https://www.cnki.com.cn/Article/CJFDTOTAL-JSKS201902006.htm.

Hari, S., Krishna, S., Gurrala, L. N., Singh, S., Ranjan, N., Rakesh Kumar Vij, R. K., Shah, S. N. (2021): Impact of reservoir, fracturing fluid and proppant characteristics on proppant crushing and embedment in sandstone formations. Journal of Natural Gas Science and Engineering 95, 104187. https://doi.org/10.1016/j.jngse.2021.104187

Ibrahim, A. F. M., Seifelnassr, A. A. S., Al-Abady, A., El-Salmawy, M. S. and Abdelaal, A. M. (2022): Characterization and Iron Removal Enhancement of El-Zaafarana White Sand. Mining, Metallurgy & Exploration, 39, 2187–2198. https://doi.org/10.1007/s42461-022-00667-0

Ibrahim, S. S., Fathy, W. M., Elsayed, M. A., Saleh, A. M., Boulos, T.R. and Moharram, M. R. (2018): An Egyptian Sandstone Deposit as a Source of Good Quality Kaolin and Ultra-Pure Silica Sand: Sample Characterization and Separation (Part I). Global Journal of Researches in Engineering: G Industrial Engineering, 18 (1), version 1.0. Online ISSN: 2249-4596 & Print ISSN: 0975-5861.

Ibrahim, S. S., Ali, S. Q. and Hagrass, A. A. (2013): Gravity Separation of Silica Sands for Value Addition. Particulate Science and Technology, 31, 590–95. https://doi.org/10.1080/02726351.2013.800930

Ibrahim, S. S., Farahat, M. M. and Boulos, T. R. (2015): Optimizing the performance of the RER magnetic separator for upgrading silica sands. Particulate Science and Technology, 35, 21-28. https://doi.org/10.1080/02726351.2015.1121179

Imarc. (2024): Frac Sand Market Size & Share | Industry Analysis Report, Outlook & Forecast 2024-2032. https://www.imarcgroup.com/frac-sand-market.

International Standardization Organization. (2015): ISO 9001, Quality management systems- Requirements. Edition 5. 29 pages.

ISO 13503-2:2006 Petroleum and natural gas industries -- Completion fluids and materials -- Part 2: Measurement of properties of proppants used in hydraulic fracturing and gravel-packing operations

Jia, X., Liu, R., Ren, H., Han, Y., Ouyang, J., Zheng, H., Peng, C. and Zheng, J. (2022): Particle shape characterizations for energetic materials by computational geometry and stereology method. SN Applied Sciences 4, 147. https://doi.org/10.1007/s42452-022-05031-x

Kong, J., Jin, X., Liu, Y., Wei, D., Jiang, S., Gao, S., Feng, Z., Xing, P. and Luo, X. (2019): Study on the kinetics of iron removal from silicon diamond-wire saw cutting waste: Comparison between heterogeneous and homogeneous reaction methods. Separation and Purification Technology 221, 261–268. https://doi.org/10.1016/j.seppur.2019.03.069

Krumbein, W. C. (1941): Measurement and Geological Significance of Shape and Roundness of Sedimentary Parti-

cles. Journal of Sedimentary Petrology 11, 2, 64-72. https://doi.org/10.1306/D42690F3-2B26-11D7-8648000102C1865D

Krumbein, W. C. and L. L. Sloss. (1963): Stratigraphy and sedimentation. Edition 2. W.H. Freeman and Company, San Francisco, 660 pages.

Laarhoven, B.V., S.H. Schaafsma, S.H., G.M.H. Meesters (2012): Towards a desktop attrition tester; validation with dilute phase pneumatic conveying. Chemical Engineering Science 73, 321-328. https://doi.org/10.1016/j.ces.2011.08.038

Liang, F., Sayed, M., Al-Muntasheri, G. A., Chang, F. F., Li, L. and others. (2016): A comprehensive review on proppant technologies. Petroleum 2, 26-39. https://doi.org/10.1016/j.petlm.2015.11.001

Liang, T., Zhang, J., Meng, C., Xiu, N., Cai, B. and Fu, H. (2020): Conductivity prediction of proppant-packs based on particle size distribution under variable stress conditions. 2nd International Conference on Energy Geotechnics (ICEGT 2020). E3S Web Conference 205. https://doi.org/10.1051/e3sconf/202020503010

Liu, C., Wang, W., Wang, H., Zhu, C. and Ren, B. (2023): A Review on Removal of Iron Impurities from Quartz Mineral. Minerals 13, 1128. https://doi.org/10.3390/min13091128

Liu Y., Mu, S., Guo, J., Chi, C., Wang, S. (2021): Model for fracture conductivity considering particle size distribution in a proppant monolayer. Journal of Natural Gas Science and Engineering 95, 104188. https://doi.org/10.1016/j.jngse.2021.104188

Manda Okar, A. (2024): Market Research Future. info@marketresearchfuture.com.

Nigussie, A., Demisse, T., Getaneh, W. (2023): Industrial properties and uses of silica sand from Blue Nile Basin, Central Ethiopia. Arabian Journal of Geosciences 16(3), 213. https://doi.org/10.1007/s12517-023-11302-7

Mocciaro, A., Lombardi, M. B., Scian, A. N. (2018): Effect of raw material milling on ceramic proppants properties. Applied Clay Science 153, 90-94. https://doi.org/10.1016/j.ces.2011.08.03810.1016/j.clay.2017.12.009

O'Driscoll, M. (2015): Proppant Prospects for Industrial Minerals. SME 2015. Denver, Colorado, Feb 15-18.

Othman, N., Mustaffar, M. I., Ismail, S. A. and Ibrahim, M. H. (2023): Upgrading silica rock quality by using attrition scrubbing and magnetic separation techniques. Materials Today: Proceedings. https://doi.org/10.1016/j.matpr.2023.04.659

Powder & Bulk Solids (2019): Frac Sand Prices Forecast to Remain Flat Through 2024. https:// www. powderbulksolids.com> mining- metals.

Ravisankar, V., Wu, J., Bhargava, S. and Parthasarathy, R. (2023): Studying particle attrition in a solid-liquid agitated vessel using focused beam reflectance measurement. Chemical Engineering and Processing, Process Intensification 183, 109256. https://doi.org/10.1016/j.cep.2022.109256

Research and Markets (2024): 2024 Silica Sand Market Outlook Report: Industry Size, Market Shares Data, Insights, Growth Trends, Opportunities, Competition 2023 to 2031.

Sanchez, D., Gilchrist, D., Yang, S., Bandara, K., Gamage, R. and Zheng, W. (2022): Experimental characterization of time-dependent mechanical behaviours of frac sand at high compressive stresses and implication on long-term proppant conductivity. Geomechanics and Geophysics for Geo-Energy and Geo-Resources Journal 8, 85. https://doi.org/10.1007/s40948-022-00398-y.

The Business Research Company (2024): Silica Sand Global Market Report. Published Jan. 2024. inbound@tbrc.info

Ulusoy, U. (2023): A Review of particle shape effects on material properties for various engineering applications: From macro to nanoscale. Minerals 13, 91. https://doi.org/10.3390/min13010091.

Wadell, H. (1932): Volume, shape, and roundness of rock particles. The Journal of Geology 40, 443–51. https://www.jstor.org/ stable/30058012.

Wadell, H. (1935): Volume, shape and roundness of quartz particles. The Journal of Geology 43, 250.

Wahab, G., Ibrahim, G. and Abdel Wahab, A. (2022): Geological and engineering appraisal of hydraulic frac sand in some Egyptian localities as a proppant of oil well drilling. Heliyon 8, e10233. https://doi.org/10.1016/j.heliyon.2022.e10233

Wu, T., Zhou, J., and Wu, B. (2019): HF/HCl acid resistance mechanisms of alumina ceramics in the Al2O3-MgO-CaO-SiO2-Y2O3 system. Ceramics International 45, 4455–60. https://doi.org/10.1016/j.ceramint. 2018.11.124

Zheng, J. and Hryciw, R. D. (2015): Traditional soil particle sphericity, roundness and surface roughness by computational geometry. Géotechnique 65, 494–506. https://doi.org/10.1680/geot.14.P.192

Zheng, W. and Tannant, D. (2016): Frac sand crushing characteristics and morphology changes under high compressive stress and implications for sand pack permeability. Canadian Geotechnical Journal 53. https://doi.org/10.1139/cgj-2016-0045

Zheng, J. and Hryciw, R. D. (2017): Soil Particle Size and Shape Distributions by Stereophotography and Image Analysis. Geotechnical and Testing Journal 40, 317-328. https://doi.org/10.1520/GTJ20160165

Zheng, W., Costa Silva, S., Tannant, D.D. (2018): Crushing characteristics of four different proppants and implications for fracture conductivity. Journal of Natural Gas Science and Engineering 53, 125-138. https://doi.org/10.1016/j.jngse.2018.02.028

Zheng, W., Hu, X., Tannant, D. and Zhou, B. (2021): Quantifying the influence of grain morphology on sand hydraulic conductivity: a detailed pore-scale study. Computers and Geotechnics 135, 104147. https://doi.org/10.1016/j.compgeo.2021.104147

Zoveidavianpoor, M., Gharibi, A. (2016): Characterization of agro-waste resources for potential use as proppant in hydraulic fracturing. Journal of Natural Gas Science and Engineering 36, 679-691. https://doi.org/10.1016/j.jngse.2016.10.045

SAŽETAK

## Poboljšanje kvalitete silikatnoga pijeska kao propanta za potrebe hidrauličkoga frakturiranja

Uzorak silikatnoga pijeska iz kamenoloma *Egypt's Future Quarries*, koji se nalazi jugozapadno od Kaira, ispitivan je za korištenje kao propant tijekom hidrauličkoga frakturiranja. Iako se pokazalo da uzorak ima dobra fizička i mehanička svojstva, bilo je potrebno poboljšati njegove karakteristike kako bi odgovarao specifikacijama Međunarodne organizacije za standardizaciju. Nakon pregleda mikroskopom i utvrđivanja mineraloškoga sastava glavnoga uzorka predložena je shema jednostavnoga i jeftinoga oplemenjivanja, uključujući klasifikaciju prosijavanjem i tehniku oplemenjivanja trošenjem korištenjem uređaja Denver kapaciteta 50 L. Rezultati su pokazali znatno poboljšanje kvalitete oplemenjenoga pijeska. Sadržaj silicijeva oksida ($SiO_2$) porastao je s 90,10 % na 98,15 % nauštrb oksida aluminija i željeza koji su smanjeni za 79 % odnosno 63 %. Ovo poboljšanje kvalitete naknadno je dovelo do znatnoga poboljšanja u mjerama zamućenosti i topljivosti u kiselini te je na taj način uzorak pijeska iz neprihvatljivoga za industriju nafte i plina pretvoren u proizvod s prihvatljivim specifikacijama za tu industriju. Rezultati su također pokazali poboljšanje u otpornosti na drobljenje (24,06 %), sferičnosti (19,11 %) i zaobljenosti zrna (16,72 %). Osim toga, granulometrijski sastav pijeska nakon postupka trošenja pokazao je veću konzistentnost, što je za propant poželjno.

**Ključne riječi:**
hidrauličko frakturiranje, karakteristike propanta, silikatni pijesak, čišćenje pijeska trošenjem

## Author's contribution

**Suzan S. Ibrahim (1)** (Professor Emeritus of Mineral Processing Technology Dept. at CMRDI, Cairo) participated in developing the idea of the research, planned and developed the work plan, followed up on the experimental work, and wrote the research. **Tawfik R. Boulos (2)** (Professor Emeritus of Mineral Processing Technology Dept at CMRDI, Cairo) came up with the idea for the research, participated in providing important scientific references, and carried out the final scientific review of the research manuscript. **Sameh M. Abdullah (3)** (works at Concord for Engineering and Contracting, M.Sc. candidate at TIMS) provided the silica sand technological sample and participated in most of the experimental work. **Abdalla M. Elbendari (4)** (PhD, a researcher, Mineral Processing Technology Dept. at CMRDI) participated in conducting, monitoring and analyzing the attrition scrubbing operations and the measurements of the shape of sand particles concerning sphericity and roundness using a Mega Pixels 1600x 8 Led digital electronic microscope. **Mohamed G. Khalifa (5)** (Professor Emeritus of Metallurgy at TIMS) followed up on all parts of the scientific work of the research and participated in the final review of the manuscript. **Ayman A. Hagrass (6)** (PhD, a researcher at TIMS) participated in developing the work plan for the research, conducting and participating in most of the research experiments and scientific discussions, as well as in collecting the scientific references for the research.